

## MASS AND MOMENTUM TURBULENT TRANSPORT EXPERIMENTS

B. V. Johnson  
United Technologies Research Center  
East Hartford, Connecticut 06040

An experimental study of mixing downstream of coaxial jets discharging in an expanded duct was conducted (1981) to obtain data for the evaluation and improvement of turbulent transport models currently used in a variety of computational procedures throughout the propulsion community for combustor flow modeling. The study used laser velocimeter (LV) and laser induced fluorescence (LIF) techniques to measure velocities and concentration and flow visualization techniques to qualitatively determine the time dependent characteristics of the flow and the scale of the turbulent structure.

Qualitative and quantitative studies were conducted of the flow downstream of coaxial jets discharging into an expanded duct. The ratio of annular jet diameter and duct diameter to the inner jet diameter were .2 and 4, respectively. The inner jet peak velocity was approximately one-half the annular jet peak velocity. Results from the studies were related to the four shear regions within the duct: (1) wake region downstream of the inlet, (2) shear layer between the jets, (3) recirculation region, and (4) reattachment region.

Flow visualization studies were conducted using dye as a trace material and high-speed motion pictures to record the dye patterns in selected  $r-z$  and  $r-\theta$  planes. The principal results from this study showed:

1. The larger scales of the turbulent structure were observed to grow from the width of the wake region downstream of the inner jet tube to a large fraction of the duct diameter immediately upstream of the reattachment zone.
2. The turbulent eddies were not axisymmetric or periodic at any location within the duct. The large scale waves and eddies appeared to have a range of wave lengths.

A detailed map of the velocity, concentration, mass transport rate and momentum transport rate distribution within the duct was obtained to provide data for the evaluation and improvement of turbulent transport models. Data sets of two velocity components pairs were obtained simultaneously to determine momentum transport rate and velocities. Data sets of velocity and concentration pairs were obtained simultaneously to determine mass transport rate, concentration, and velocity. Probability density functions (p.d.f.s) of all the forementioned parameters were

obtained from the data sets. Mean quantities, second central moments, skewness and kurtosis were calculated to characterize each data set. The principal results from this study are:

3. The axial and radial velocity profiles documented the changes in the shear regions within the duct.

4. The mean and fluctuating concentration profiles documented the inner jet fluid distribution within the duct.

5. The turbulent momentum transport rate measurements in the r-z plane documented the local momentum fluxes due to turbulent mixing. Correlation coefficients were determined for each measurement location and data set.

6. Countergradient turbulent axial mass transport was measured in the shear region between jets. The peak axial mass transport rates were greater than the peak radial mass transport rates even though the axial concentration gradients were approximately one-fifth the radial gradients.

7. The countergradient turbulent axial mass transport was related to the general direction of the eddies between the inner and annular jets. The countergradient axial mass transport occurred when the annular jet was accelerating the inner jet fluid.

8. The skewness and kurtosis of the momentum transport p.d.f.s in the peak shear region were approximately the same as previously measured in turbulent boundary layers. However, the kurtosis in the low shear region was greater than previously measured in the wake region of the turbulent boundary layers.

9. The peak values of kurtosis for the mass transport p.d.f.s was greater than the peak values for the momentum transport p.d.f.s.

10. The kurtosis for all the transport rate p.d.f.s were an order of magnitude greater in the low transport rate regions, including the recirculation region, than in the high transport rate regions.

Report: Mass and Momentum Turbulent Transport Experiments with Confined Coaxial Jets by B. V. Johnson, J. C. Bennett, NASA Contractor Report NASA CR-165574, November 1981.

Currently swirling coaxial jets are being experimentally studied using the same LV/LIF measurement technique used in the nonswirling coaxial jet study. The only change in the flow condition from the previous study is the addition of 30 deg mean angle swirl to the annular jet fluid. The flow visualization technique has been improved to show interaction of shear layers on both sides of the annular stream.

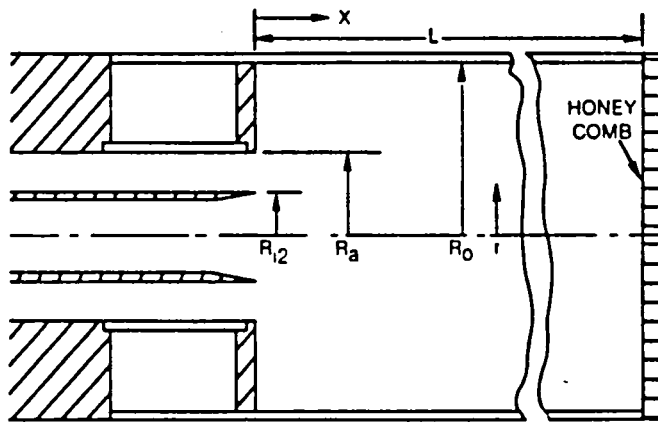


Figure 1. Sketch of inlet and test section;  $L = 1016$  mm,  
 $R_{i1} = 12.5$  mm,  $R_{i2} = 15.3$  mm,  $R_a = 29.5$  mm,  
 $R_0 = 61.0$  mm.

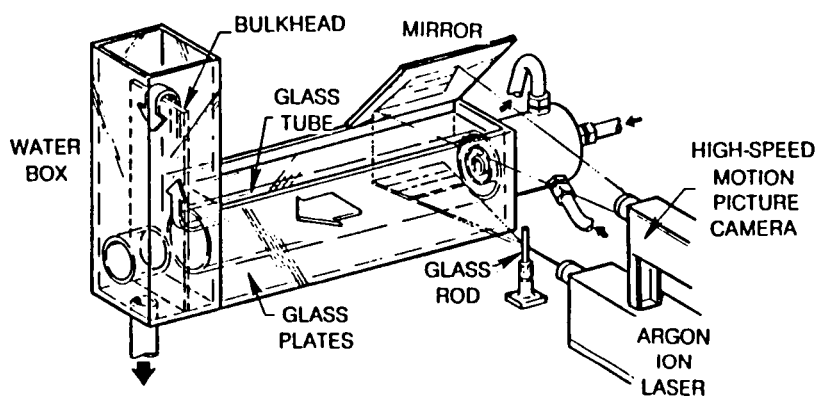


Figure 2. Optical arrangement for flow visualization in  $r$ - $z$  plane.

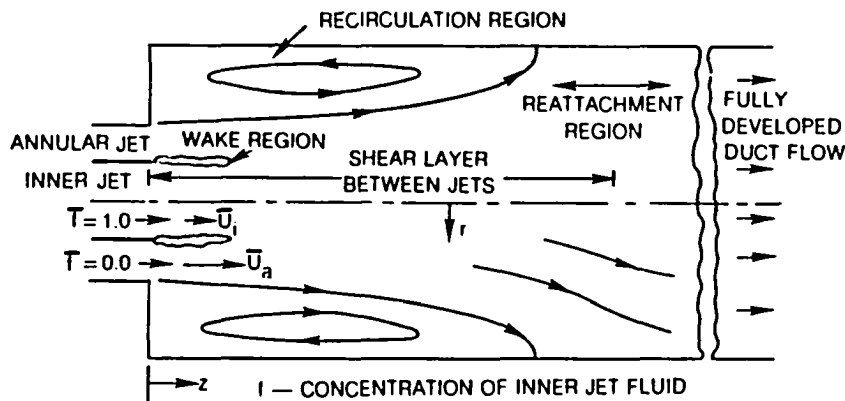


Figure 3. Shear regions of nonswirling coaxial jets in an enlarged duct.

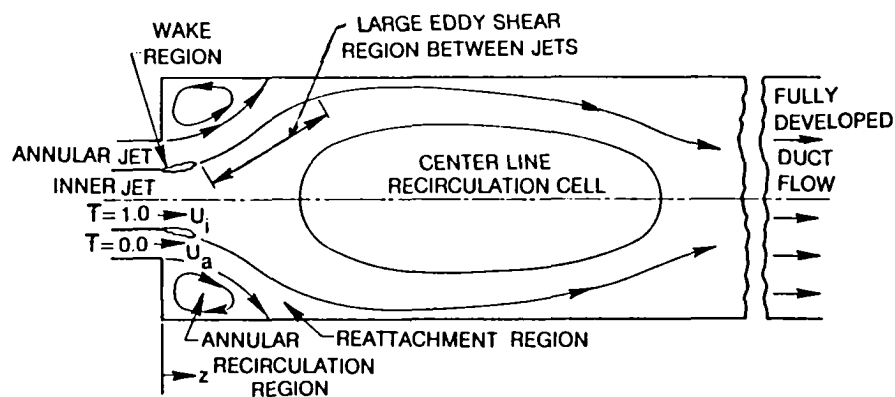


Figure 4. Shear regions of coaxial jets with swirl in an enlarged duct.

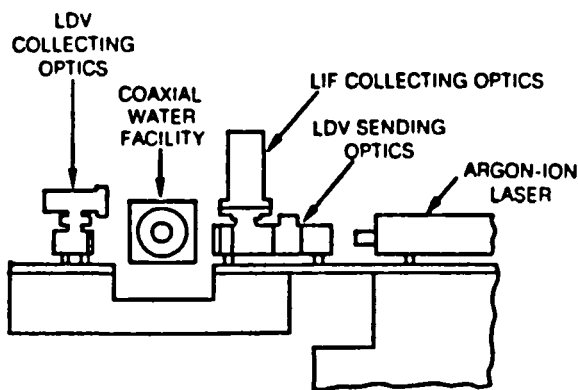


Figure 5. Sketch of optics arrangement.

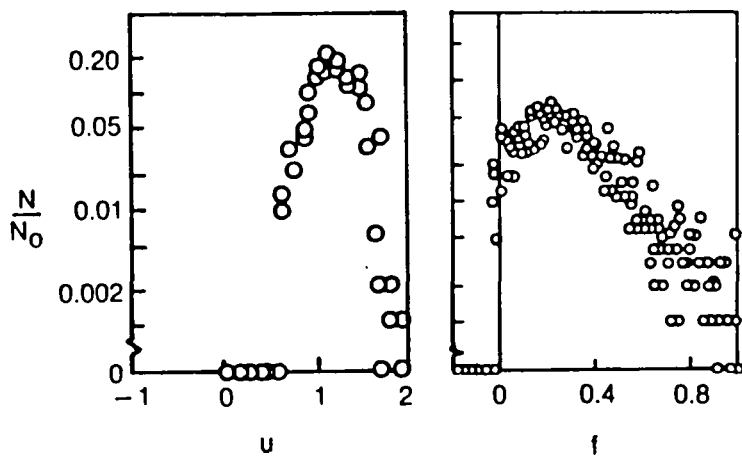


Figure 6. Probability density functions for axial velocity and concentration at  $r/R_0 = 0.2$ ;  $\Delta u = 0.1$  m/s,  $\bar{u} = 1.20$  m/s,  $u' = 0.22$  m/s,  $S_u = -0.15$ ,  $K_u = 216$ ;  $\Delta f = 0.02$ ,  $\bar{f} = 0.28$ ,  $f' = 0.18$ ,  $S_f = 0.91$ ,  $K_f = 4.0$ .

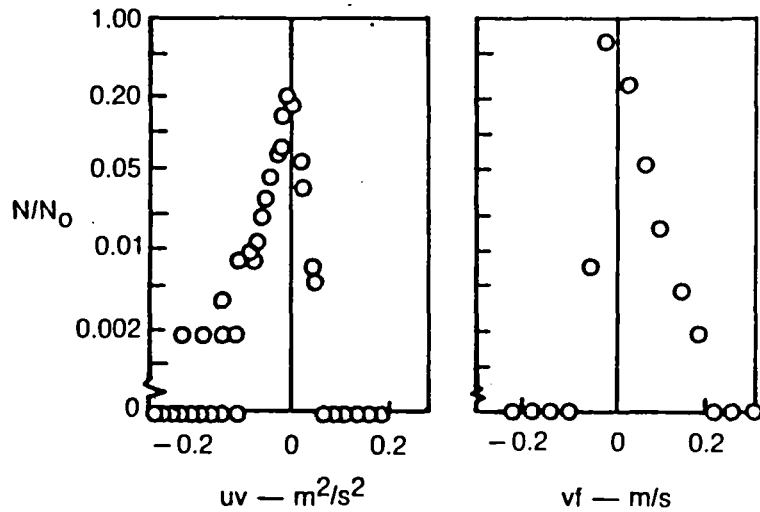


Figure 7. Probability density functions for r-z momentum and radial mass transport ratio at  $r/R_0 = 0.2$ ;  $\Delta uv = 0.01 m^2/s^2$ ,  $\bar{uv} = 0.0142 m^2/s^2$ ,  $\sigma_{uv} = 0.030 m^2/s^2$ ,  $S_{uv} = -2.14$ ,  $K_{uv} = 11.9$ ;  $\sigma_{vf} = 0.04 m/s$ ,  $\bar{vf} = 0.0165 m/s$ ,  $\sigma_{vf} = 0.028 m/s$ ,  $S_{vf} = 2.23$ ,  $K_{vf} = 10.4$ .

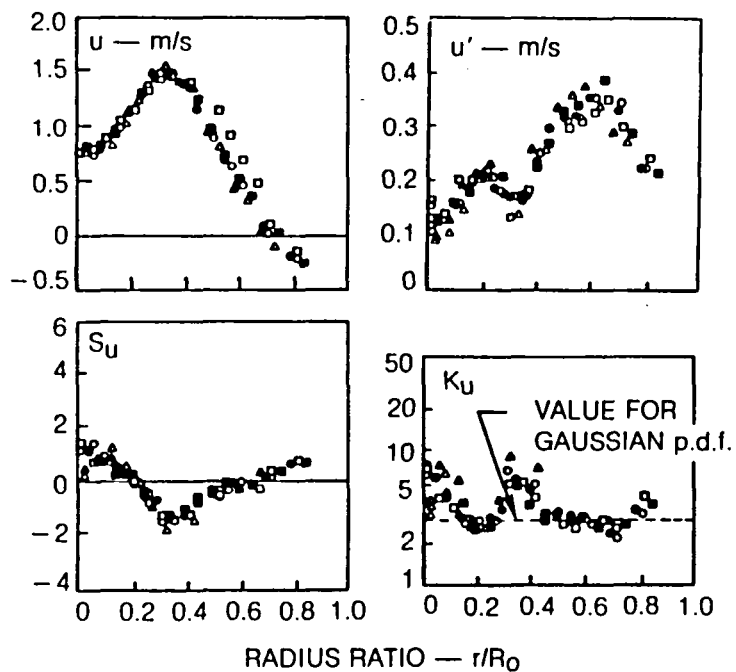


Figure 8. Moments of axial velocity profile;  $0 = 0$  deg -  $\Delta$ ,  $180 = \bullet\Delta$ ,  $90 = \blacksquare$ ,  $270 = \square$ .

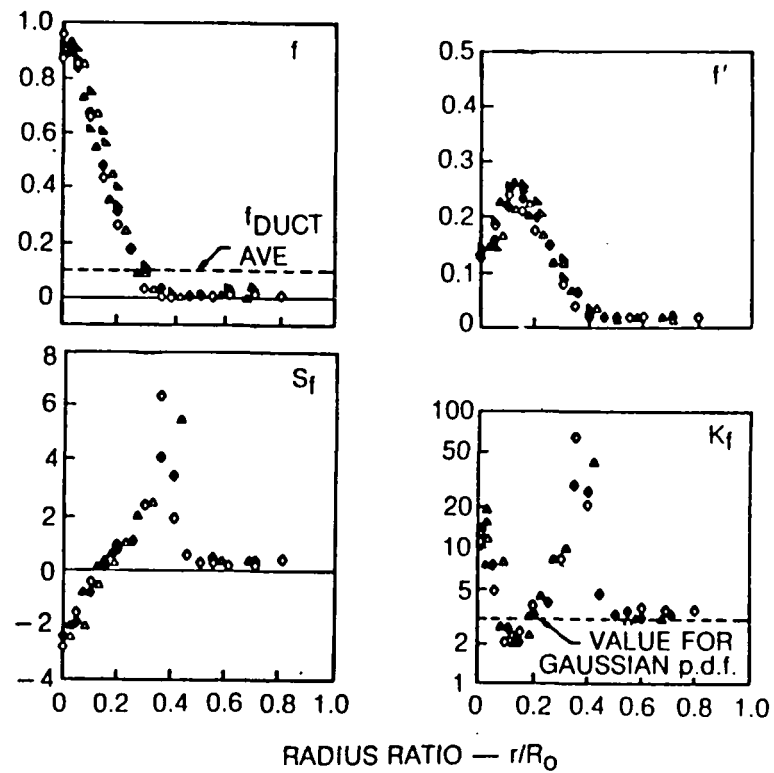


Figure 9. Moments of concentration profiles;  $0 = 0$  deg -  $\Delta$ ,  $180$  -  $\blacktriangle$ ,  $90$  -  $\blacklozenge$ ,  $270$  -  $\lozenge$ .

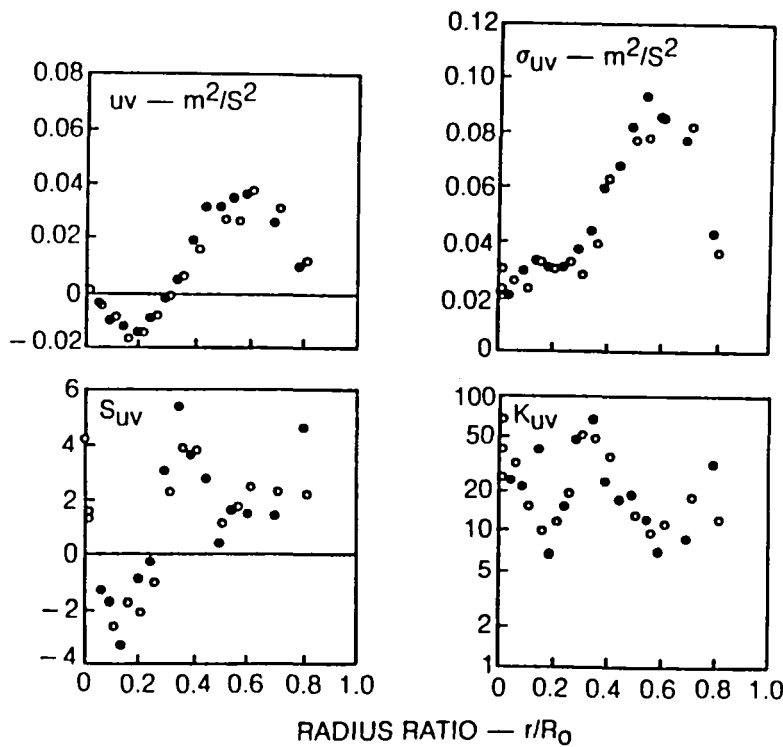


Figure 10. Moments of turbulent momentum transport profiles;  
 $0 = 0$  deg -  $\circ$ ,  $180$  -  $\bullet$ .

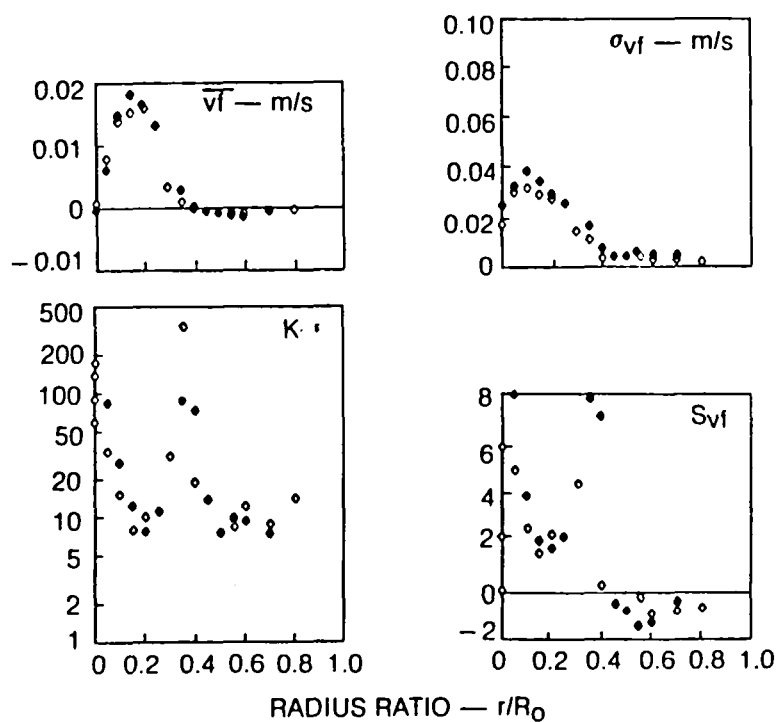


Figure 11. Moments of turbulent radial mass transport profiles;  $0 = 0$  deg -  $\diamond$  ,  $180$  -  $\blacklozenge$  .

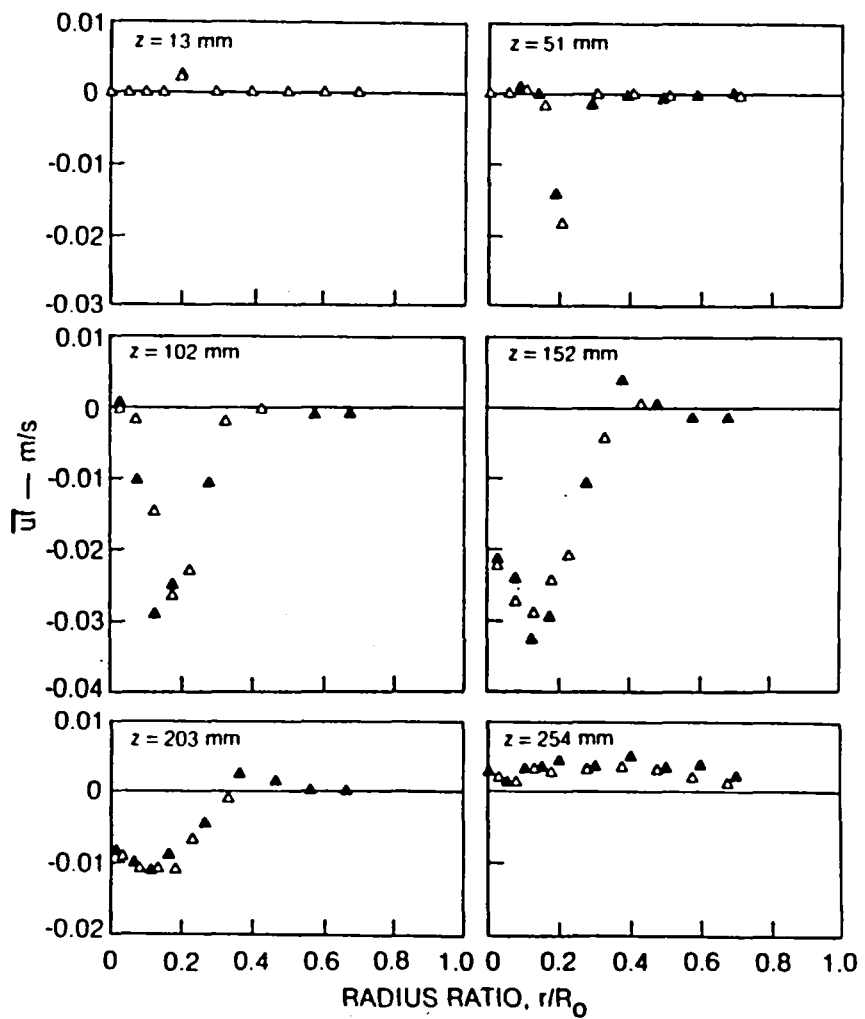


Figure 12. Axial mass transport rate profiles;  $\circ = 0 \text{ deg}$   $-\Delta = 180 \text{ deg}$ .

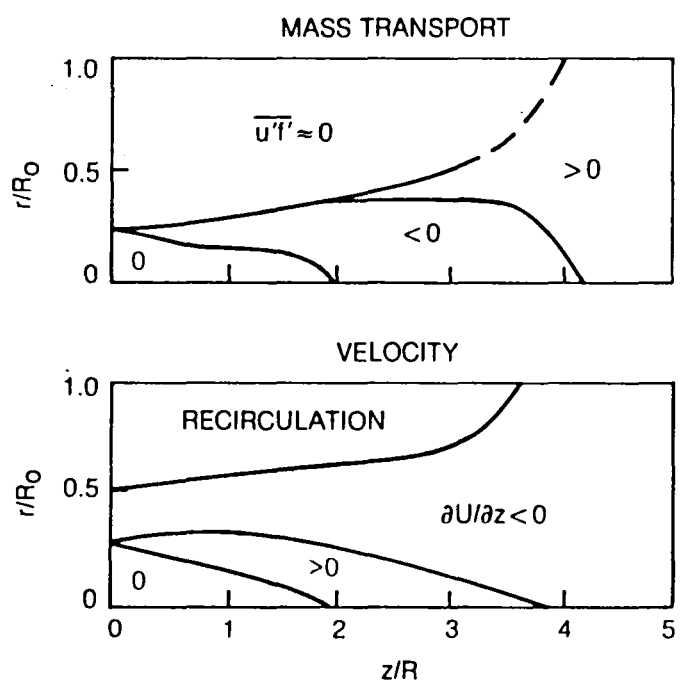


Figure 13. Regions of countergradient axial mass transport and axial velocity accelerations;  $\overline{u'f'} < 0$  is countergradient region.